PAPER

Check for updates

Wound healing efficacy of curcumin-loaded sandalwood bark-derived carbon nanosphere/PVA nanofiber matrix†

M. Roopesh,[a] Deljo Davis,[b] M. S. Jyothi,[c] M. Vandana, [b] B. S. Thippeswamy,[d] Gurumurthy Hegde, [*e] T. P. Vinod [b] and Rangappa S. Keri [*a]

The present investigation deals with the evaluation of the wound healing efficacy of sandalwood bark-derived carbon nanospheres loaded with curcumin-embedded polyvinyl alcohol (PVA) nanofiber membranes (NF). Carbon nanospheres (CNS) were prepared by pyrolyzing sandal wood bark powder at 750 °C. The morphology was confirmed by field emission scanning electron micrographs and a rich amount of carbon was confirmed by the energy dispersive X-ray technique. Curcumin, an active wound healing drug was loaded onto synthesized CNS and confirmed by ATR-IR studies. Drug-loaded CNS were anchored in a PVA matrix *via* electrospun nanofiber fabrication. The fabricated nanofiber membranes were characterized and evaluated for wound healing efficiency. The cytotoxicity assay proved the non-toxic nature of the prepared PVA/CNS-curcumin-loaded NF. Membranes with active CNS/drug showed better antimicrobial activity against *S. aureus* and *E. coli*, which was estimated using the zone of inhibition (ZOI) test. The *in vitro* scratch wound healing assay of prepared PVA/CNS-curcumin nanofibers was efficient enough and showed 92 to 98% wound closure, which was greater than the control (without drug) nanofiber membranes. The PVA nanofiber matrix with interconnected structure and carbon nanostructures together enhanced the wound healing efficacy of the considered wound healing membrane, which is a promising novel approach for future wound healing patches.

1. Introduction

The human body's greatest vital organ, the skin serves as the first line of defense against foreign microbes.[1] Nevertheless, external forces such as burns, cuts, surgical operations, and ulcers damage the skin layer and the degree of damage varies with the type, depth, and maintenance of the injury and skin. The damaged skin is recovered by tissue regeneration with four different stages, such as hemostasis, inflammation, proliferation, and remodelling.[2] Though skin regeneration is

ᵃOrganic and Medicinal Chemistry Laboratory, Centre for Nano and Material Sciences, Jain (Deemed-to-be University), Jain Global Campus, Kanakapura, Jakkasandra Post, Kanakapura Road, Ramanagara District, Bangalore, Karnataka, India – 562112. E-mail: keriphd@gmail.com; sk.rangappa@jainuniversity.ac.in; Tel: +918027577199

ᵇDepartment of Chemistry, CHRIST (Deemed to be University), Bhavani Nagar, Hosur Road, Bengaluru 560029, India

ᶜDepartment of Chemistry, AMC Engineering College, Bannerughatta Main Road, Bengaluru-560083, India

ᵈDepartment of Biomedical Science, College of Pharmacy, Shaqra University, Al-Dawadmi Campus, Kingdom of Saudi Arabia

ᵉCentre for Advanced Research and Development (CARD), CHRIST (Deemed to be University), Bhavani Nagar, Hosur Road, Bengaluru 560029, India. E-mail: murthyhegde@gmail.com; Tel: +91-7019202135

† Electronic supplementary information (ESI) available. See DOI: https://doi.org/10.1039/d3ra04181f

a complicated process, a certain degree of spontaneity in its repair is observed, however, depending on the surrounding environment. In the management of wound healing, wound dressings are crucial. They expedite the healing process and shield the wound from external dangerous factors.[3] Traditional dressings have not been able to satisfy the needs of the current market due to their inadequate antibacterial potential and other flaws, despite the rising need for wound care and treatment globally.

For an ideal wound dressing, in addition to absorbing excess exudate, these materials should also be non-toxic, biocompatible, degradable, maintain a moist healing environment at the wound site, facilitate gas exchange, protect the wound from microbial infection, stimulate angiogenesis, and tissue regeneration.[4–6] The most popular dressings available right now are primarily made of film, hydrogels, sponge, and nanofiber (NF) membranes. The NF membranes with unique structure, size, and porosity, these membranes defend the wound from infections and even allow feasible gas and liquid molecules transportation. Especially, electrospun NF membranes possess a high surface-to-volume ratio and versatility, due to which they are employed in several pharmaceutical applications such as drug delivery, tissue engineering, and wound dressing.[7–10] Electrospun NF membranes have the structural similarity with natural extracellular matrix (ECM) that proposes an epitomic

microenvironment offering cell adhesion, cell multiplication, and migration.[11,12] In addition, the porous nature and the interconnected network of NF would essentially create the microenvironment required for swift wound healing. The structure would also allow the intercalation or loading of bioactive ingredients, which further enhances the healing process.

Numerous initiatives involving drug-loaded NF membranes have been documented, especially using biodegradable scaffolds and natural bioactive components. Cardamom extract was anchored in the electrospun NF fabricated with a combination of sodium alginate and polyvinyl alcohol (PVA).[13] The web loaded with 86% of cardamom extract was released at 144 h and showed a promising antimicrobial effect and wound dressing ability. A combination of aloe vera,[14] and curcumin[15] with chitosan and polycaprolactone, PVA/chitosan/starch,[16] and others[17–20] were attempted for various kinds of wounds. The drugs were loaded into nanoparticles such as ZnO, TiO_2, silver and many carbon-based nanoparticles,[20,21] and are in trend for wound healing applications. The synergy between the electrospun network and the nanoparticles leads to a sustained release of the drug and enhanced antimicrobial potential.[22]

Our previous reports highlighted curcumin loading onto TiO_2 nanoparticles[23] and oil palm leaves derived CNS[24] for effective wound dressings. With a glance at the literature and the motivation for the previous works, the present work emphasizes the usage of carbon nanospheres (CNS) prepared using the sandalwood bark waste via pyrolysis as a potent drug carrier. The porous CNS were loaded with curcumin and embedded in a biodegradable electrospun PVA NF network, characterized and examined for wound healing efficacy via in vitro scratch wound healing assay and in vivo excision wound healing model.

2. Materials and methods

2.1 Materials

Sandal wood bark waste was collected from the Western Ghats statue makers shop. Curcumin was obtained from Vidya Herbs, India. Polypropylene non-woven support was purchased from local vendors, in Bengaluru. Other chemicals such as PVA, phosphate buffer (PBS), ethanol, and dimethyl sulfoxide (DMSO) were procured from Merck, India. The agar medium for antimicrobial studies was purchased from Thermo Fischer Scientifics. MTT reagent, DMEM high glucose, and fetal bovine serum (FBS) were from Himedia, bacteria such as *Escherichia coli* and *Staphylococcus aureus* were procured from Microbial Type Culture Collection (MTCC) and Gene Bank, Chandigarh.

2.2 Synthesis of SWCNS

The collected fresh sandalwood bark (SW) pieces were washed thoroughly in deionized water to remove surface dust particles. The pieces were dried under sunlight and finely powdered using the ZM200, RETSCH, Germany, ultra-centrifuge mill at 12 000 rpm and sieved to ∼60–65 microns with a laboratory sieve shaker. Uniform sieving is essential to obtain uniform

nanoparticles in the later stages. CNS was then synthesized via pyrolysis using a tube furnace (obtained from NoPo Nanotechnologies Pvt Ltd, Bangalore) at 750 °C for two hours in a continuous flow of N_2 gas. Care should be taken to avoid the oxygen flow otherwise it is difficult to obtain high-quality carbon nanospheres.

2.3 Drug loading to SWCNS

100 mg of SW bark-derived CNS was dispersed in ethanol of 50 ml and sonicated for 20 min. An equal amount of Cur (100 mg) was added to the mixture, sonicated for 15 min, and stirred for 5 h. The mixture was kept undisturbed for 24 h and vacuum filtered to obtain Cur-loaded CNS. The excess Cur was removed by giving a thorough wash to the obtained solid with distilled water and dried to get curcumin-loaded CNS. The obtained product will be addressed as Cur/CNS for convenience.

2.4 Fabrication of SWCNS/PVA nanofibers

The homogeneous (1%, w/v) dispersion of CNS was prepared by sonicating the CNS–water mixture for 20 min using a probe sonicator. Care should be taken to disperse the nanoparticles uniformly in the solution so as to get a highly dispersed solution for the later stage studies. PVA was dissolved in the CNS–water mixture at 10%, w/v concentration by heating to 75 °C under magnetic stirring to obtain a homogeneous solution. This solution was subjected to electrospinning to obtain PVA-CNF. For electrospinning, the solution was filled in a 5 ml syringe attached with a needle of diameter 0.8 mm. For the electrospinning process, the syringe tip was kept 12 cm away from the drum collector, which was covered with non-woven fabric. Electrospinning was carried out with a flow rate of 0.05 ml h^{-1} and an applied voltage of 25 kV while the drum collector was rotating with a speed of 350 rpm. Bare PVA NF, curcumin-loaded PVA, and Cur/CNS-loaded PVA NF were also prepared using the same procedure. Hereafter, bare PVA, PVA loaded with CNS, PVA loaded with curcumin, and PVA loaded with Cur/CNS are referred to as PVA, PVA-C, PVA-D, and PVA-CD, respectively.

2.5 Characterization techniques

Synthesized SWCNS and fabricated wound healing membranes were characterized by various microscopic and spectroscopic techniques. The crystalline nature of the materials was observed through X-ray diffraction (XRD) using a Model D8 Advance: Bruker AXS, Germany, from a 2θ of 10° to 80°, with a step size of 0.02° and scan rate of 0.5° min^{-1} was employed to confirm the compositions. A Bruker ECO-ATR-IR (Attenuated Total Reflectance-Infrared) spectrophotometer with a wave number ranging from 400 cm^{-1} to 4000 cm^{-1} was used to analyse the surface functionalities of used drugs, carbon particles, and also fabricated membranes.

The surface morphological analysis was carried out using a field emission scanning electron microscope (FESEM), FESEM JSM-7001F model. For FESEM analysis, a current of 10–10 A and a voltage of 5.0 kV was applied. The membranes were sputter coated with gold before analyzing. For prepared membranes, the basic surface morphology was analyzed by the optical

profilometer KLA Tencor ZETA-20. The hydrophilic nature of the membrane surface was confirmed by contact angle measurements using a digital microscope and digital viewer.

2.6 Wettability tests

Membranes of 5 cm × 2 cm size were cut and placed in a hot air oven for 24 h at 37 °C to remove extra moisture and dry weights were recorded. Then, the samples were placed in 10 ml distillation water. After 24 h, the samples were taken out and wiped with tissue paper to remove extra water, and weights were recorded using analytical grade balance. Water uptake (%) was calculated (eqn (1)) by comparing with initial weight, the samples were studied in triplicates, and results are represented with mean values.

$$\text{water uptake}\% = \left(\frac{M - M_o}{M_o} \right) \times 100 \qquad (1)$$

where M is the weight of the wound dressing membrane after swelling at time t and M_o is the weight of the dry wound dressing membrane.

2.7 Cytotoxicity assay

In vitro cell viability or the cytotoxicity of the curcumin-encapsulated SWCNS was examined by a standard colorimetric MTT (thiazolyl blue tetrazolium bromide) assay. MTT was dissolved in 5 mg ml⁻¹ in PBS and then any formazan crystals formed were removed by filtration. The prepared solution was stored at −20 °C and considered as a stock solution, dilution of which in the ratio 1 : 10 was used as a working solution. 3T3-L1 cells were employed for the study. 100 μl/1000 cells were plated in a 96-well plate and incubated for 48 h under a 5% CO_2 atmosphere at 37 °C. 100 μl of the sample solution prepared from powders were added to each plate, cells with only media were referred to as control. The plates were incubated again in a CO_2 atmosphere for 24 h at 37 °C. The medium was removed and MTT (100 μl) was added to each well and incubated for 2 h. The cells were washed and collected using DMSO. Formazan crystals formed were analyzed using spectrophotometry at 570 nm.

2.8 Antibacterial activity

Escherichia coli and *Staphylococcus aureus*, two different Gram-positive and Gram-negative bacteria, were used in the antibacterial test for fabricated wound dressings. A disc-shaped membrane with a diameter of 12 mm was placed on the LB agar medium in a Petri dish and inoculated with 10^5 CFU ml⁻¹ of cell concentration. The plates were incubated for 24 hours at 37 °C after being refrigerated for 1 hour to allow proper diffusion. Each membrane's zone of inhibition (ZOI) was measured using a Vernier calliper.

2.9 *In vitro* wound healing activity

To study *in vitro* wound healing activity, a scratch wound healing assay was utilized. At first, the cells were grown in DMEM with high glucose media supplemented with 10% FBS until the

cells reach 70–80% confluence. The cells were seeded into 12 well tissue culture plates at a density of 0.25 million cells per well until they reach ~80–100% confluence as a monolayer for the incubation period of 24 h. The monolayer was gently scratched with a 200 μl pipette across the center of the well and the second scratch was performed perpendicular to the first by making a cross in each well. The wells were gently washed with the medium to remove the detached cells. Fresh media was added and incubated at 37 °C with 5% CO_2. Fabricated wound dressings were UV sterilized for 30 min and 2 mg of each film sample was dissolved in 1 ml of DMEM media with FBS and kept in a gyratory shaker for 24 h to secrete the active bio-components present in the films to surrounding media and media was used for the assay. The cells were grown from 24 to 48 h and the images were captured at different time intervals (0, 24, and 48 h). The pictures were taken at different views of the monolayer multiple times for accurate results.

2.10 Animals and *in vivo* wound healing activity

Six-week-old male Sprague Dawley rats were kept in individual housing with free access to water and a regular chow diet. Every animal was kept on a 12 hour dark/light cycle. Animals were randomly divided into four equal groups with six animals in each group. Group I was treated with PVA, Group II was treated with PVA-C, Group III was treated with PVA-D, and Group IV was treated with PVA-CD membrane. The experiments were performed according to the guidelines of the institutional animal ethics committee (IAEC, SSCP/203/2019-20), Sree Siddaganga College of Pharmacy, Tumkuru, Karnataka.

Animals were given an intraperitoneal injection of a combination of ketamine and xylazine of 70 mg kg⁻¹ and 10 mg kg⁻¹ before having their dorsal skin shaved. A tail pinch was used to measure the depth of anaesthesia. On the animal's depilated dorsal thoracic region, a predetermined area of wound of around 2 cm² was produced in an aseptic environment. Analgesics were given to treat the pain and anxiety. The membranes were positioned on the created wound facing the active surface towards the wound. The wounds were wrapped with crape bands and individually housed. On days 7 and 14, skin regeneration and wound healing were assessed together with sham control and infection control. The area of the wound was measured on the day it was created by drawing the limits of the wound on a piece of translucent paper. On a graph piece of paper, the wound locations in each group were noted. On each dorsal excision site covered with sterile surgical gauze, wound dressing membranes were applied in accordance with the experimental design specifications. From the day that the wound area was measured and the skin tissue underwent histology, the percentage of the wound's contraction and epithelization phase was examined.

2.11 Histopathology

On the fourteenth day of the investigation, skin samples were obtained and histograms were examined. Full-thickness cross-sectional skin samples were gathered and tested for histopathological changes.

3. Results and discussion

3.1 Characterization of sandalwood bark-derived CNS

A practical and safe pyrolysis process without a catalyst was used to create CNSs in a green manner. To determine the initial shape and mass ratios of carbon and other elements, SEM (Fig. 1a) and EDX (Fig. 1b) inspections of the precursor sandalwood bark were performed. Carbon accounted for 94.06% of the elemental makeup, and oxygen made up 5.94%. Calcium (Ca) and silicon (Si) in negligible levels were also confirmed. The average sphere size from the SEM image ranged from 30 to 50 nm, as shown in Fig. 1a. The sandalwood structure and coarse porosity can act as a precursor for the development of CNSs without the use of either catalysts or templates. CNS's XRD pattern (Fig. 1c) showed one peak that is connected to the microcrystalline structure of carbon. Surprisingly, CNSs showed an extremely small peak at 2 theta = 23.20° corresponding to the 120 plane. This peak might have been caused by the cellulose and hemicellulose properties of sandalwood bark, which are extremely crystalline. Because of the highly graphitic nature of CNSs, the XRD analysis points to the emergence of a novel class of carbon nanomaterial. As a result, XRD tests further emphasized the high carbon content of the sandalwood bark, as shown from the other analysis. When determining the graphitic properties of carbon nanomaterials, Raman spectroscopy is incredibly helpful. The two main peaks in the carbon materials are D-bands, which indicate structural disorder within the carbon network, and G-bands, which indicate structural order. The D-band was seen at 1341.3 cm^{-1} in the current CNSs, which were produced at 750 °C for pyrolysis (Fig. 1d). The G-band, which is associated with the sp^2 bound carbon atom from stretching modes of C=C bonds and corresponds to the E$_{2g}$ mode of graphite, was present in the CNSs at a wavelength of 1601.9 cm^{-1}. The I_d/I_g ratio was found to be 0.837, which can both be used to determine the graphitic character.

These findings led us to create nanoparticles at a 750 °C pyrolysis temperature, which helped to create highly organized CNSs. Although not ideal, these temperatures are sufficient to demonstrate the materials' potential. To examine the impacts of rising temperatures in these directions, more research is being performed.

3.2 Characterization of nanofiber membranes

Synthesized PVA NF membranes (PVA alone, PVA with only drug (PVA-D), PVA with drug-loaded CNS (PVA-CD), and PVA with CNS (PVA-C)) were characterized using FESEM, XRD, and ATR-IR studies. FESEM micrographs of PVA, PVA-C, and PVA-CD nanofiber membranes are presented in Fig. 2. In all three cases the nanofiber nature was retained. A revisit to the literature confirmed that the nanofiber matrix acted as an ECM and showed exclusive biological functions. The retained nanofiber structure is expected to potentially encapsulate the drug and deliver the active substances promoting the healing process.[25] However, there were some clots observed for PVA-CD
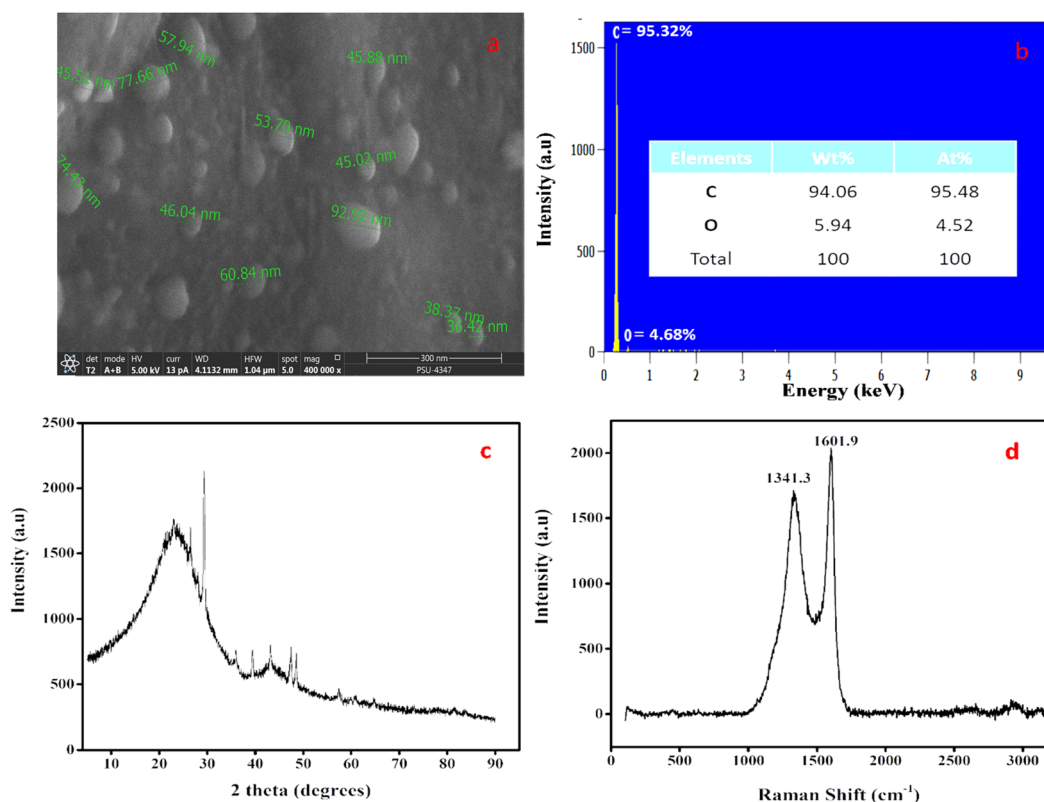
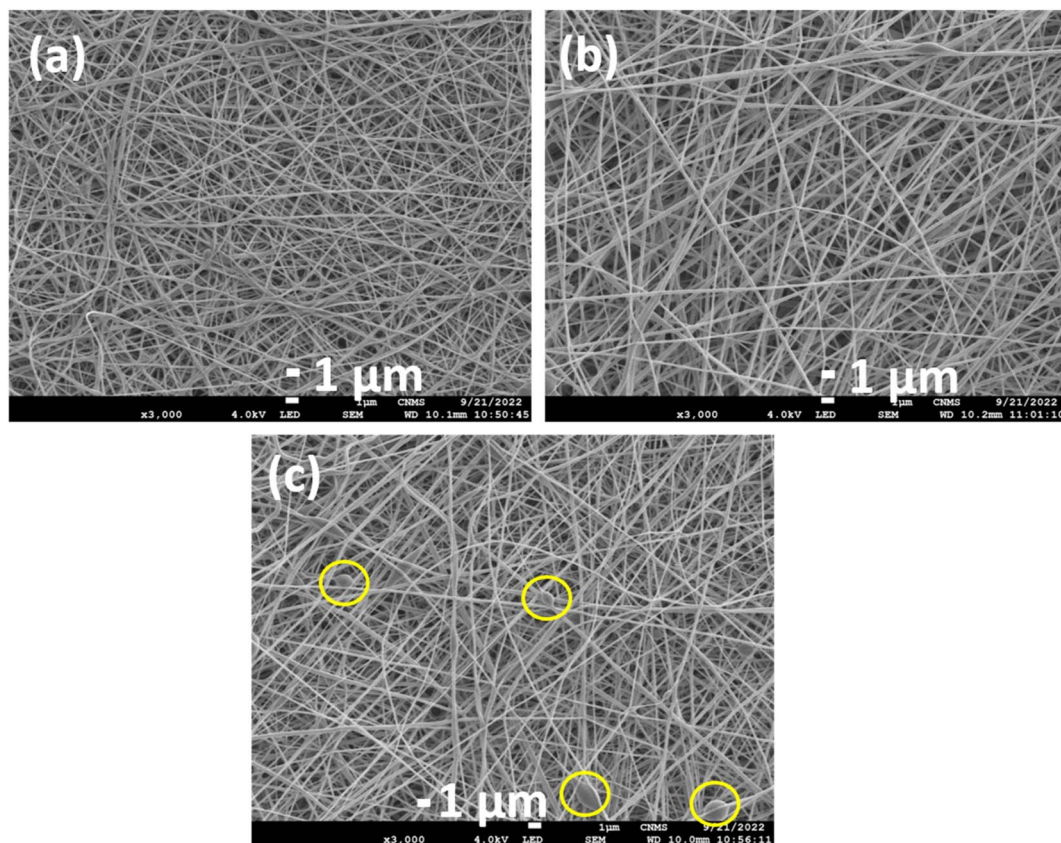**Fig. 1** (a) FESEM; (b) EDS; (c) XRD and (d) RAMAN studies of the sandalwood bark-derived carbon.

Fig. 2 FESEM micrographs of (a) PVA NF; (b) PVA–C NF and (c) PVA–CD NF membranes (the inset circles of (c) present the formation of agglomerates).
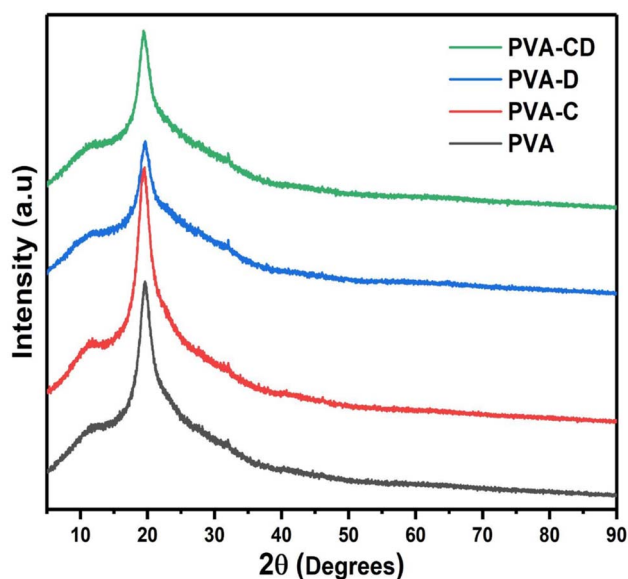

Fig. 3 XRD patterns of PVA, PVA–CD, PVA–D and PVA–C.

The impact of CNS loading and the CNS/drug loading on the crystallinity of the PVA matrix was analysed from the XRD measurements and the results are shown in Fig. 3. A single peak at $2\theta = 18.7°$ was obtained, which is a characteristic peak for the

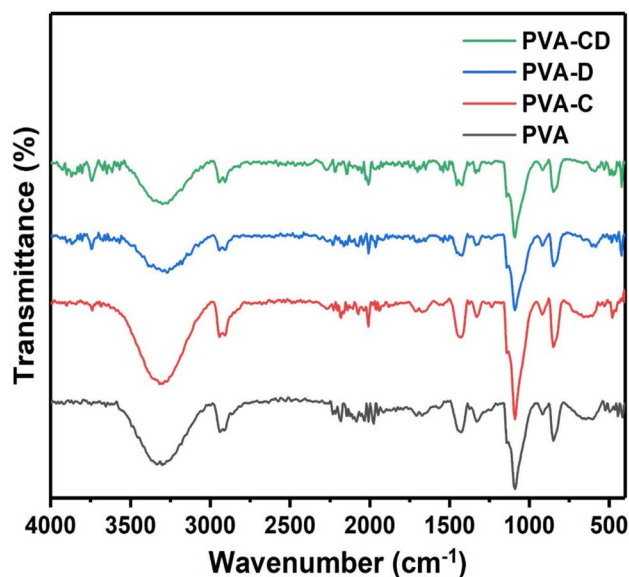**Fig. 4** ATR-IR spectra of PVA, PVA–CD, PVA–D, and PVA–C.

membranes (highlighted in circles, Fig. 2c), which are attributed to the uneven evaporation during the spinning process, due to the varied affinity of drug-loaded carbon nanospheres and PVA towards the solvent used for membranes fabrication.
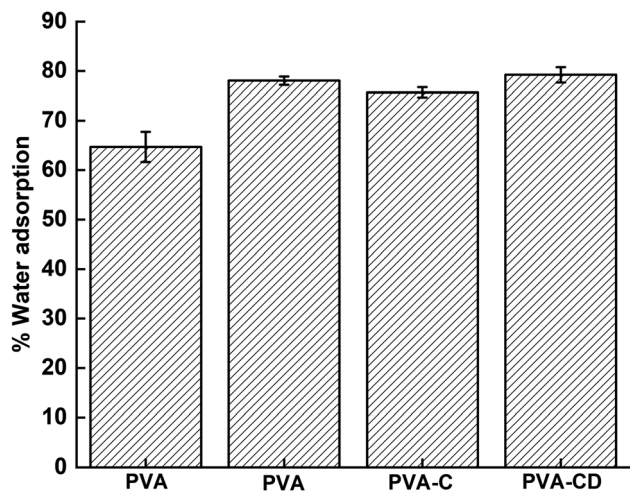
Fig. 5 Water adsorption capacity of PVA, PVA-D, PVA-C, and PVA-CD nanofiber membranes.
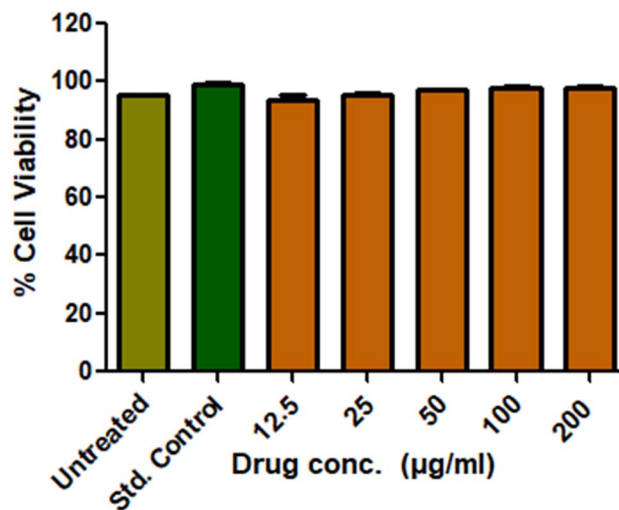

Fig. 7 Cell viability test for drug-loaded SW-derived CNS.

crystalline PVA matrix.[26] The peak was observed for all other three matrixes as well and also, confirming the retained crystallinity even after drug and CNS loading. The ATR-IR of the fabricated membranes is presented in Fig. 4. The $C=O$ stretching of PVA nanofibers was obtained at 1000 to 1320 cm^{-1}.[27] The hydroxyl group of PVA gave peaks at 3250 to 3400 cm^{-1} and 910 to 950 cm^{-1}.[28] C–H–C–H peaks were observed at 610–700 cm^{-1} and $C=O$ peaks were seen at 1665–1710 cm^{-1}.[29] Several variable bands of $C=H$ bond were observed at 1450–1470 cm^{-1}. The peaks were observed for all other nanofibers as well. The peaks of Cur and the CNS are predicted in similar ranges, however, slight changes are observed for the drug-loaded or CNS-loaded membranes.

3.3 Wettability of the membranes

Wettability is one of the significant parameters for wound healing applications, as the healing process depends on moisture content and air content at the surface. The wettability of the membranes obtained using the immersion method is provided in Fig. 5 and the contact angle measurement results are provided in Fig. 6. PVA is known as a hydrophilic material and showed water absorption of 77%. With the addition of CNS, drug, and drug-loaded CNS, the water adsorption capacity increased further, due to the porous nature and the

functionalities provided by the filler materials. However, no significant alterations were observed with the addition of fillers, which was also supported by contact angle measurements. The contact angle of PVA and PVA-C almost remained the same, highlighting the fact that CNS had no contribution in increasing the surface hydrophilicity of PVA NF. However, the membranes involving drug molecules showed lower contact angle values (53.3° and 54.1° for PVA-D and PVA-CD, respectively) indicating the contribution of curcumin towards increased hydrophilicity when compared with PVA and PVA-C.

3.4 Cytotoxicity test

Cytotoxicity is crucial for the wound healing membranes, which decides the biocompatibility of the same. The L929 cell lines were used to investigate the cytotoxicity of the prepared CNS-loaded drug material *via* the MTT assay. The live cells produce mitochondrial lactate dehydrogenase, which reduces MTT and forms insoluble formazan crystals. These crystals gave a peak at 570 nm under UV-visible spectroscopy. Obtained results are provided in Fig. 7. The untreated cell lines gave around 96% cell viability and the std. control gave around 98.7%. The drug-loaded CNS was given to cell lines at varied concentrations. Acceptable cell viability up to 98% was observed at all the concentrations owing to their biocompatibility and their candidature towards biological applications.
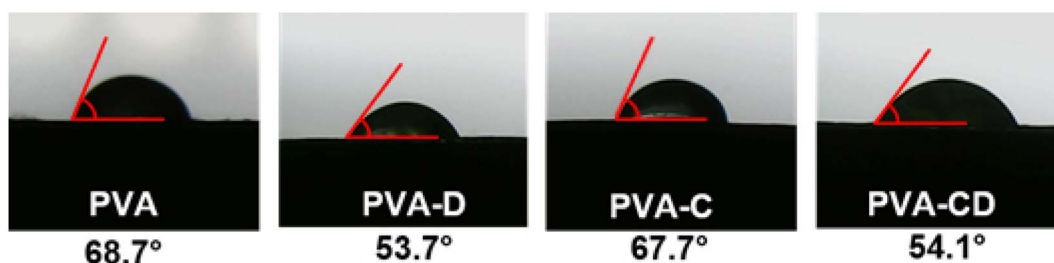

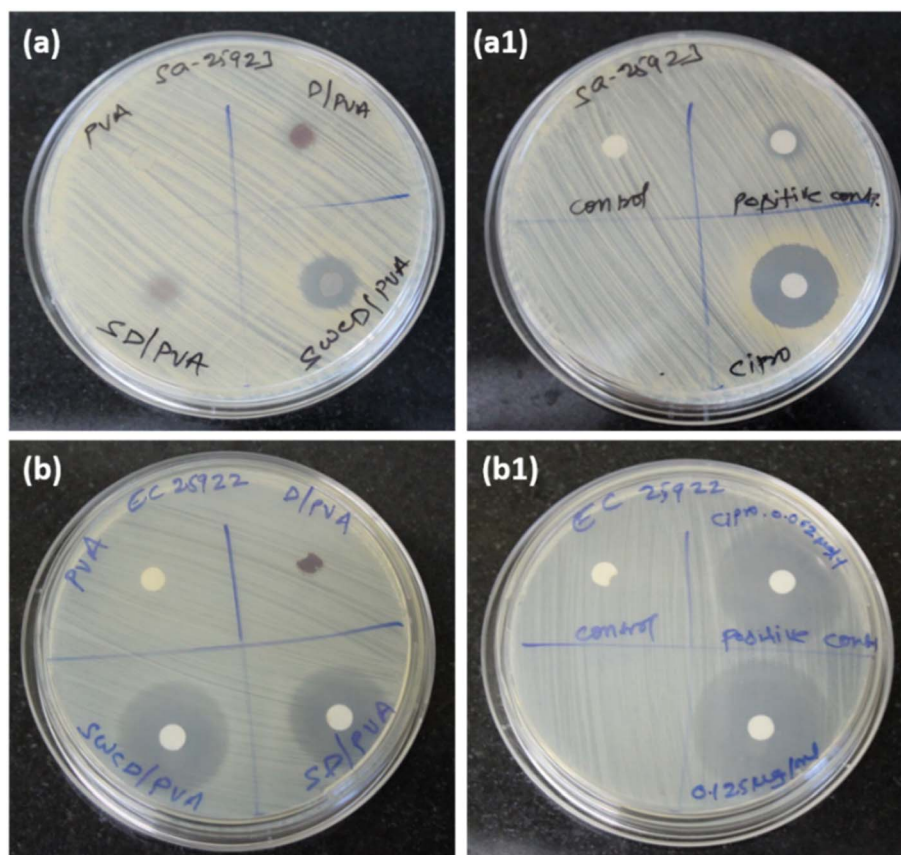Fig. 6 Water contact angle measurements for PVA, PVA-D, PVA-C, and PVA-CD.

Fig. 8 Antimicrobial assay for (a) PVA, PVA-D, PVA-CD, SWCD/PVA and (a1) control, positive control and ciprofloxacin against *S. aureus*; (b) PVA, PVA-D, PVA-CD, SWCD/PVA and (b1) control, positive control and ciprofloxacin against *E. coli*.

3.5 Antibacterial test

The antimicrobial efficacy of synthesized NFs was tested against *S. aureus* and *E. coli* along with the standard drug ciprofloxacin. The results of the ZOI test performed are presented in Fig. 8 and Table 1. Fig. 8a and b both did not show ZOI for PVA alone and a good value of ZOI was observed against *E. coli* than *S. aureus*. PVA-CD, which is mentioned as SWCD/PVA in the figures presented a maximum ZOI of 16.5 and 32.4 mm for *S. aureus* and *E. coli*, respectively. The permeability and integrity of bacterial cell membranes in both Gram-positive and -negative bacteria can be damaged by curcumin, according to studies, which ultimately results in bacterial cell death. Because of curcumin's lipophilic nature, it can enter liposome bilayers directly, increasing the permeability of the bilayer.[30] Curcumin is also known to induce reactive oxygen species (ROS) mediated cell death leading to an apoptosis-like response in bacterial cells, which would further result in cell membrane depolarization as well as increased Ca^{2+} influx.[31] The standard drug ciprofloxacin-treated plates presented the concentration-dependent ZOI. The carbon nanostructure is proven to possess antibacterial activity[32] and a similar trend has been observed. However, the PVA matrix with curcumin-loaded nanospheres presented better ZOI than the others. As *E. coli* possess a more soft surface than *S. aureus*,[33] maximum antibacterial activity was observed for *E. coli* and the results are comparable with those from standard drug ciprofloxacin.

3.6 *In vitro* wound healing activity

The concerned biological application was investigated *via in vitro* wound healing efficiency. The scratch wound assay results for wound healing efficiency of fabricated membranes against L929 cells at 0, 24, and 48 hours are provided in Fig. 9. The cell proliferation was almost similar for the standard control and the considered final material PVA-CD-treated cells at 24 hours. PVA, PVA-C, and PVA-D also showed cell proliferation, however, the migration was less. The covered wound area overlay is presented in Fig. 10. For untreated cells at 0 hours, 721 588.8 μm area was observed and it was 672 259.2 μm for PVA-CD treated cells. The same for 48 hours was 4981.6 μm. While the standard control showed 7280.8 μm. All

Table 1 Obtained zone of inhibition values for PVA, PVA-D, PVA-C, and PVA-CD against *S. aureus* and *E. coli* along with ciprofloxacin

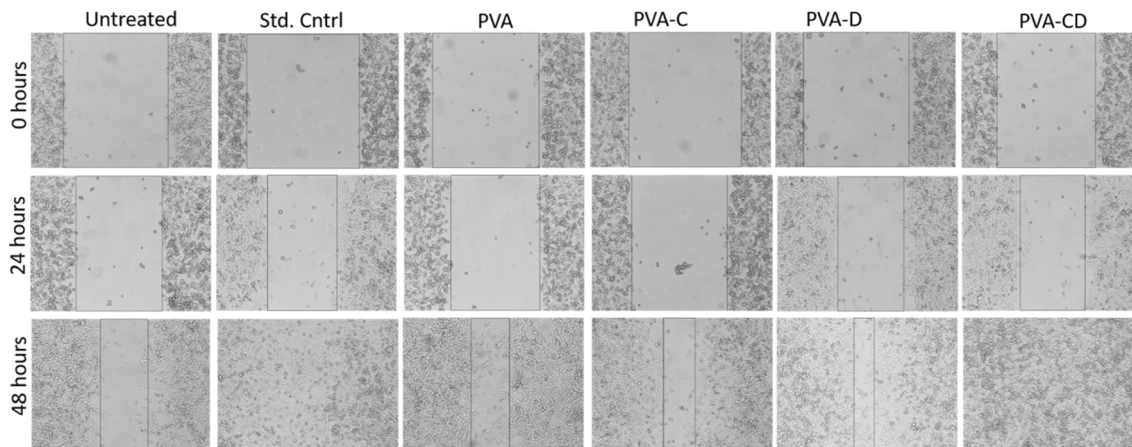|	Average ZOI (mm)					
	Test compounds				Ciprofloxacin	
Organisms	PVA	PVA-D	PVA-C	PVA-CD	0.25 μg ml^{-1}	0.5 μg ml^{-1}
S. aureus	No ZOI	8.3	10.3	16.5	5.3	23.5
E. coli	No ZOI	5.2	25.4	32.4	26.7	37.4

Fig. 9 *In vitro* L929 wound healing of untreated, std. control, drug, PVA, 5% drug + PVA membranes, and 10% drug + PVA treated cells with respect to time.
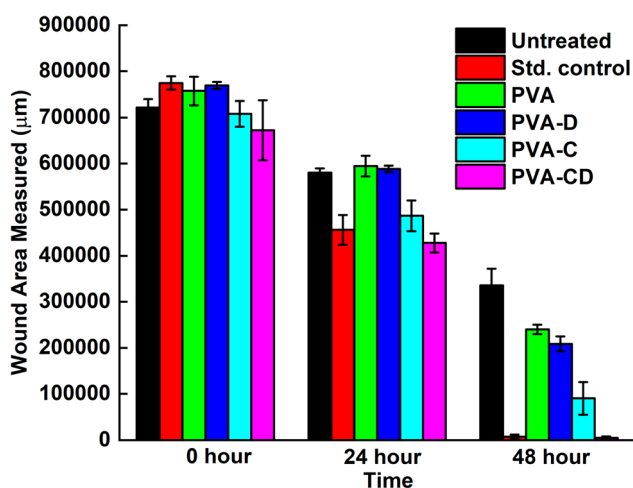

Fig. 10 Wound area covered overlay for L929 cells.

other cells (PVA, PVA-C, and PVA-D) showed greater wound coverage.

The percentage of wound closure was calculated for the scratch wound healing assay and the results are presented in terms of % cell migration v/s time in Fig. 11 and the figure facts are presented in Table 2. The % wound closure was maximum for standard control and was minimum for untreated cells at 24 hours. Nevertheless, at 48 hours. The % wound closure for both the standard control and PVA-CD-treated drug was 99% at 48 hours.

Surprisingly, PVA-C-treated cells showed greater % wound closure (87.22%) than PVA-D (72.89%) treated cells. The wound closure results confirmed the efficacy of curcumin for PVA-D by 26% and for PVA-CD by 46%.

3.7 *In vivo* wound healing efficacy

The *in vivo* wound healing efficacy of prepared PVA NF membranes (PVA, PVA-C, PVA-CD, PVA-D) was examined using an excision wound model. The camera pictures of the wounds

on 0th day, 7th day, and 14th day are presented in Fig. 12. The PVA-treated wound showed very less wound closure (~56%) on the 14th day of the treatment. PVA-C and PVA-D membranes treated wounds showed ~84 to 88% wound closure. Whereas, the one treated with PVA-CD presented ~99% wound closure. The CNS acted as efficient curcumin carriers, and synergy
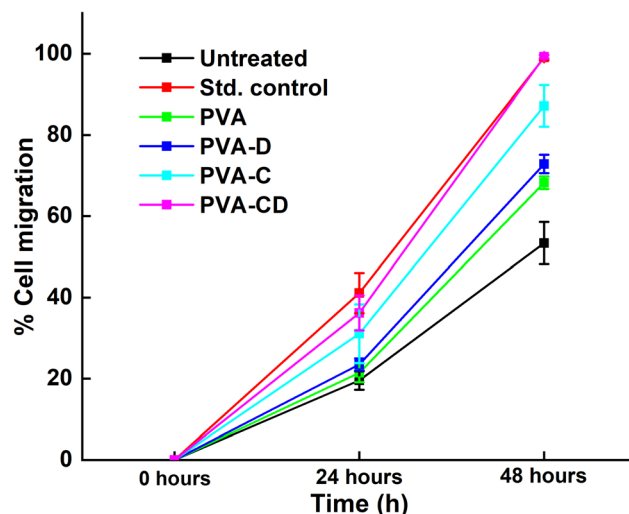

Fig. 11 Percentage of wound closure for considered drug and membranes at three different time points.

Table 2 Percentage of wound closure scored for considered drug and drug-loaded membranes

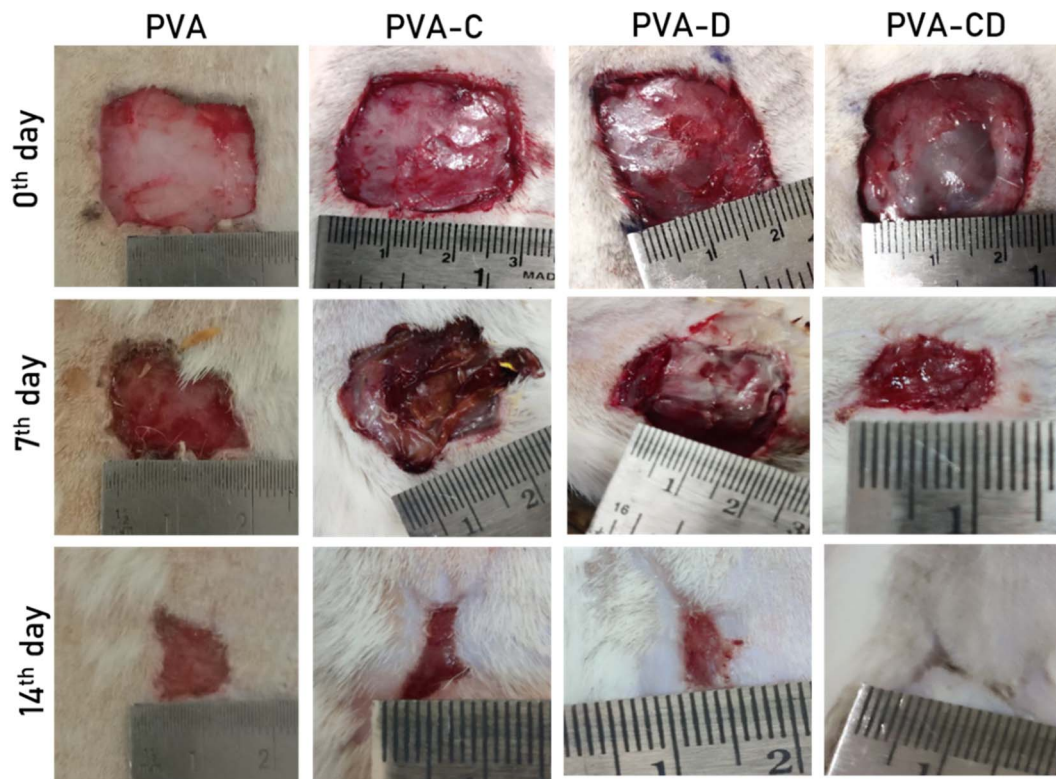| Overlay of % wound closure scored			
Incubation time (h)	0	24	48
Untreated	0	19.5748 ± 2.28	53.4268 ± 5.19
Std. control	0	41.1362 ± 4.97	99.0597 ± 0.65
PVA	0	21.4914 ± 2.31	68.2670 ± 1.57
PVA-D	0	23.4940 ± 1.47	72.8921 ± 2.24
PVA-C	0	31.2989 ± 7.23	87.2234 ± 5.07
PVA-CD	0	36.4445 ± 4.29	99.2589 ± 0.44
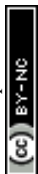
Fig. 12 The camera pictures of wounds of considered animals treated with PVA, PVA-C, PVA-D, and PVA-CD on 0th, 7th, and 14th days of the treatment.
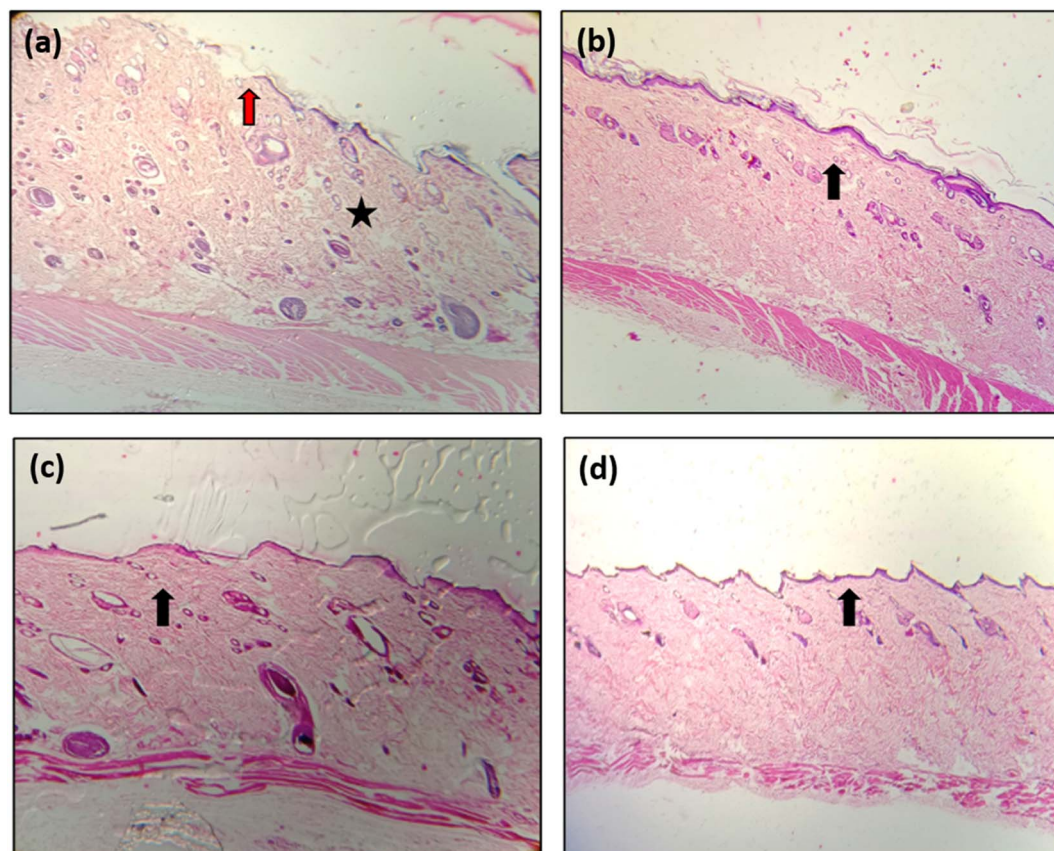

Fig. 13 Histograms of skin tissues of wounds treated with (a) PVA, (b) PVA-C, (c) PVA-D, (d) PVA-CD.

between the curcumin drug and the PVA nanofiber matrix resulted in excellent wound healing.

3.8 Histopathology

On day 14th of the treatment, the skin tissue samples were subjected to histopathological evaluation, and the histograms are presented in Fig. 13. An infiltration of cell particulars and the poor re-epithelization of skin tissue were observed for the PVA-treated wound skin. A considerable increase in the reepithelization was observed for wounds treated with PVA NF having curcumin (PVA-D) and CNS (PVA-C). However, with decreased infiltration of cell particulars and increased tissue regeneration, re-epithelization was achieved for the wound treated with PVA-CD (PVA NF matrix having curcumin-loaded CNS).

4. Conclusions

Sandalwood bark was pyrolyzed at 750 °C to obtain carbon nanospheres. The obtained CNSs were loaded with drug molecules (curcumin). Wound-healing PVA membranes were fabricated *via* the electrospinning technique. The incorporation of drug molecules and CNS did not affect the fibrous nature of the fabricated membranes, which further helped the efficient wound healing process. The MTT assay showed minimal toxicity and bio-compatibility of the PVA-CD membrane. The *in vitro* wound healing assay performed confirmed the efficient cell migrations for PVA-CD and the maximum wound closure of 99.25% (in par with standard control). The results were consistent with *in vivo* studies as well, the PVA-CD membrane gave ~99% wound closure indicating the successive and efficient drug-carrying ability of prepared CNS and the synergy of the PVA nanofiber matrix and wound healing ability of curcumin. The work opens a way for exploring different polymer matrixes and various drugs for the wound healing process. Also, the efficacy of the present work drives the hope of scaling up and commercialization aspects.

Animal ethical clearance

All animal procedures were performed in accordance with the Guidelines for Care and Use of Laboratory Animals of "Sree Siddaganga College of Pharmacy" University and experiments were approved by the Animal Ethics Committee of "SSCP/203/2019-20".

Conflicts of interest

There are no conflicts to declare.

Acknowledgements

References

1 I. George Broughton, J. E. Janis and C. E. Attinger, Wound healing: an overview, *Plast. Reconstr. Surg.*, 2006, **117**, 1e–32e.

2 P. Beldon, Basic science of wound healing, *Surgery*, 2010, **28**, 409–412.

3 K. Chen, F. Wang, S. Liu, X. Wu, L. Xu and D. Zhang, *In situ* reduction of silver nanoparticles by sodium alginate to obtain silver-loaded composite wound dressing with enhanced mechanical and antimicrobial property, *Int. J. Biol. Macromol.*, 2020, **148**, 501–509.

4 H. F. Selig, D. B. Lumenta, M. Giretzlehner, M. G. Jeschke, D. Upton and L. P. Kamolz, The properties of an "ideal" burn wound dressing–what do we need in daily clinical practice? Results of a worldwide online survey among burn care specialists, *Burns*, 2012, **38**, 960–966.

5 E. Rezvani Ghomi, S. Khalili, S. Nouri Khorasani, R. Esmaeely Neisiany and S. Ramakrishna, Wound dressings: current advances and future directions, *J. Appl. Polym. Sci.*, 2019, **136**, 47738.

6 H. Liu, C. Wang, C. Li, Y. Qin, Z. Wang, F. Yang, Z. Li and J. Wang, A functional chitosan-based hydrogel as a wound dressing and drug delivery system in the treatment of wound healing, *RSC Adv.*, 2018, **8**, 7533–7549.

7 J. Venugopal, Y. Zhang and S. Ramakrishna, Electrospun nanofibres: biomedical applications, Proceedings of the institution of mechanical engineers, Part N, *J. Nanoeng. Nanosyst.*, 2004, **218**, 35–45.

8 X. Zhang, L. Li, J. Ouyang, L. Zhang, J. Xue, H. Zhang and W. Tao, Electroactive electrospun nanofibers for tissue engineering, *Nano Today*, 2021, **39**, 101196.

9 K. Ye, H. Kuang, Z. You, Y. Morsi and X. Mo, Electrospun nanofibers for tissue engineering with drug loading and release, *Pharmaceutics*, 2019, **11**, 182.

10 R. Contreras-Cáceres, L. Cabeza, G. Perazzoli, A. Díaz, J. M. López-Romero, C. Melguizo and J. Prados, Electrospun nanofibers: recent applications in drug delivery and cancer therapy, *Nanomaterials*, 2019, **9**, 656.

11 I. Behere and G. Ingavle, *In vitro* and *in vivo* advancement of multifunctional electrospun nanofiber scaffolds in wound healing applications: innovative nanofiber designs, stem cell approaches, and future perspectives, *J. Biomed. Mater. Res., Part A*, 2022, **110**, 443–461.

12 S.-M. Mousavi, Z. M. Nejad, S. A. Hashemi, M. Salari, A. Gholami, S. Ramakrishna, W.-H. Chiang and C. W. Lai, Bioactive agent-loaded electrospun nanofiber membranes for accelerating healing process: a review, *Membranes*, 2021, **11**, 702.

13 S. Najafi, A. Gholipour-Kanani, N. Eslahi and S. H. Bahrami, Study on release of cardamom extract as an antibacterial agent from electrospun scaffold based on sodium alginate, *J. Text. Inst.*, 2021, **112**, 1482–1490.

14 J. Yin and L. Xu, Batch preparation of electrospun polycaprolactone/chitosan/aloe vera blended nanofiber membranes for novel wound dressing, *Int. J. Biol. Macromol.*, 2020, **160**, 352–363.

15 S. Fahimirad, H. Abtahi, P. Satei, E. Ghaznavi-Rad, M. Moslehi and A. Ganji, Wound healing performance of PCL/chitosan based electrospun nanofiber electrosprayed with curcumin loaded chitosan nanoparticles, *Carbohydr. Polym.*, 2021, **259**, 117640.

16 H. Adeli, M. T. Khorasani and M. Parvazinia, Wound dressing based on electrospun PVA/chitosan/starch nanofibrous mats: fabrication, antibacterial and cytocompatibility evaluation and *in vitro* healing assay, *Int. J. Biol. Macromol.*, 2019, **122**, 238–254.

17 Y. Agarwal, P. S. Rajinikanth, S. Ranjan, U. Tiwari, J. Balasubramnaiam, P. Pandey, D. K. Arya, S. Anand and P. Deepak, Curcumin loaded polycaprolactone-/polyvinyl alcohol-silk fibroin based electrospun nanofibrous mat for rapid healing of diabetic wound: An *in vitro* and *in vivo* studies, *Int. J. Biol. Macromol.*, 2021, **176**, 376–386.

18 M. Najafiasl, S. Osfouri, R. Azin and S. Zaeri, Alginate-based electrospun core/shell nanofibers containing dexpanthenol: a good candidate for wound dressing, *J. Drug Delivery Sci. Technol.*, 2020, **57**, 101708.

19 S. Suganya, T. Senthil Ram, B. S. Lakshmi and V. R. Giridev, Herbal drug incorporated antibacterial nanofibrous mat fabricated by electrospinning: an excellent matrix for wound dressings, *J. Appl. Polym. Sci.*, 2011, **121**, 2893–2899.

20 J. Jiang, X. Li, H. Li, X. Lv, Y. Xu, Y. Hu, Y. Song, J. Shao, S. Li and D. Yang, Recent progress in nanozymes for the treatment of diabetic wounds, *J. Mater. Chem. B*, 2023, **11**, 6746–6761.

21 Y. Hu, H. Li, X. Lv, Y. Xu, Y. Xie, L. Yuwen, Y. Song, S. Li, J. Shao and D. Yang, Stimuli-responsive therapeutic systems for the treatment of diabetic infected wounds, *Nanoscale*, 2022, **14**, 12967–12983.

22 M. Gaur, C. Misra, A. B. Yadav, S. Swaroop, F. Ó. Maolmhuaidh, M. Bechelany and A. Barhoum, Biomedical Applications of Carbon Nanomaterials: Fullerenes, Quantum Dots, Nanotubes, Nanofibers, and Graphene, *Materials*, 2021, **14**, 5978.

23 R. Marulasiddeshwara, M. S. Jyothi, K. Soontarapa, R. S. Keri and R. Velmurugan, Nonwoven fabric supported, chitosan membrane anchored with curcumin/TiO₂ complex: scaffolds for MRSA infected wound skin reconstruction, *Int. J. Biol. Macromol.*, 2020, **144**, 85–93.

24 S. JM, R. Velmurugan, G. Hegde, R. Keri and K. Soontarapa, *Evaluation of wound healing effect of curcumin loaded OPL carbon nanospheres embedded chitosan membranes*, 2022.

25 X. Liu, H. Xu, M. Zhang and D. G. Yu, Electrospun Medicated Nanofibers for Wound Healing: Review, *Membranes*, 2021, **11**(10), 770.

26 G. Nasar, M. S. Khan and U. Khalil, Structural study of PVA composites with inorganic salts by X-ray diffraction, *J. Pak. Mater. Soc.*, 2009, **3**, 67–70.

27 A. Kumar, Y. S Negi, N. K Bhardwaj and V. Choudhary, Synthesis and characterization of cellulose nanocrystals/ PVA based bionanocomposite, *Adv. Mater. Lett.*, 2013, **4**, 626–631.

28 L. Shao, J. Li, Y. Guang, Y. Zhang, H. Zhang, X. Che and Y. Wang, PVA/polyethyleneimine-functionalized graphene composites with optimized properties, *Mater. Des.*, 2016, **99**, 235–242.

29 Z. Xu, H. Zhou, S. Tan, X. Jiang, W. Wu, J. Shi and P. Chen, Ultralight super-hydrophobic carbon aerogels based on cellulose nanofibers/poly(vinyl alcohol)/graphene oxide (CNFs/PVA/GO) for highly effective oil–water separation, *Beilstein J. Nanotechnol.*, 2018, **9**, 508–519.

30 C. Dai, J. Lin, H. Li, Z. Shen, Y. Wang, T. Velkov and J. Shen, The natural product curcumin as an antibacterial agent: current achievements and problems, *Antioxidants*, 2022, **11**, 459.

31 D. Zheng, C. Huang, H. Huang, Y. Zhao, M. R. U. Khan, H. Zhao and L. Huang, Antibacterial Mechanism of Curcumin: A Review, *Chem. Biodiversity*, 2020, **17**, e2000171.

32 Z. Sadat, F. Farrokhi-Hajiabad, F. Lalebeigi, N. Naderi, M. Ghafori Gorab, R. Ahangari Cohan, R. Eivazzadeh-Keihan and A. Maleki, A comprehensive review on the applications of carbon-based nanostructures in wound healing: from antibacterial aspects to cell growth stimulation, *Biomater. Sci.*, 2022, **10**, 6911–6938.

33 R. Sonohara, N. Muramatsu, H. Ohshima and T. Kondo, Difference in surface properties between *Escherichia coli* and *Staphylococcus aureus* as revealed by electrophoretic mobility measurements, *Biophys. Chem.*, 1995, **55**, 273–277.